Theory of the alkali-metal chemisorption on metal surfaces. II.

H. Ishida
Institute for Solid State Physics, University of Tokyo, Roppongi, Minato-ku, Tokyo 106, Japan
(Received 18 May 1990)

The electronic structure of alkali-metal adlayers on metal surfaces is studied by first-principles calculations within the local-density-functional theory as a function of coverage (Θ). Hexagonal Na layers with varying lattice constants are used as adlayers, and the substrate is modeled by the semi-infinite jellium with $r_s=2$, 3, and 4. The results obtained refine upon those in a previous work where the substrate was approximated by a jellium slab [Phys. Rev. B **38**, 8006 (1988)]. In spite of the large potential lowering in the vacuum, the density of states in a Na sphere is rather insensitive to Θ, except that the atomiclike resonances at low Θ are broadened with increasing Θ because of the formation of adlayer bands. For all the substrates, the bonding-antibonding boundary with regard to the Na-jellium bonding coincides with the Fermi level at the lowest Θ, which implies that the covalency in the Na-jellium bond and the interatomic polarization term in the Na-induced dipole moment become the largest at the lowest Θ. The rapid decrease of the dipole moment at higher Θ is caused mainly by the direct Na-Na interaction due to the orbital overlap, which leads to a stronger Na—Na bond and simultaneously to a weaker Na-jellium bond, rather than by the indirect dipole-dipole interaction.

I. INTRODUCTION

Although alkali-metal adsorption on metal surfaces is one of the simplest chemisorption systems, the variety and complexity of properties that alkali-metal adlayers exhibit in the ground state as well as in the electronic excitations are outstanding.[1-4] In addition to the well-known work-function variation with coverage (Θ) (number density of adatoms), newer subjects such as the adlayer plasmons at higher Θ,[5-7] the promotion of catalytic reactions,[8-10] the large enhancement of the efficiency of the optical second-harmonic generation,[11-13] and the adatom-induced reconstruction of metal substrates[14] have drawn interest of basic and applied surface scientists into this field. Understanding of these novel phenomena needs systematic theoretical studies covering a wide range of Θ. The first breakthrough to this direction may be to clarify the ground-state electronic structure of the adlayer as a function of Θ from first principles. In the previous paper,[15] which will be referred to hereafter as I, such an attempt was made for the first time. We studied the electronic structure of Na and Li adlayers on a high-density "jellium" surface[16] within the local-density-approximation in the density-functional theory.[17,18] It was shown that the ionic adsorption model originally put forward by Gurney[19] is not sufficient to describe the adatom-substrate (A-S) bonding, and that the covalent aspect also plays an important role. Especially, it was claimed that the Θ dependence of the adatom dipole moment that leads to the well-known work-function change can be explained in terms of the polarization of the adatom charge due to the orbital mixing of adatom and substrate states better than the conventional Θ-dependent charge transfer. These interpretations were in agreement with the electronic-structure calculation of Wimmer *et al.* for Cs/W(001) at the monolayer Θ.[20,21] They found that the Cs—W bonding is polarized covalent and that the dipole moment on a Cs site is induced via the hybridization of the Cs 6s and W 5d states. Recent experiments[22-24] also support the model deduced from these later first-principles calculations.

The drawback of the calculational method in I was in the use of a jellium slab as a substrate. This approximation replaces the continuum one-electron energy spectrum of the semi-infinite surface in the surface normal direction by discrete levels. The interaction of these levels and adsorbate states resulted in artificial spiky peaks in the calculated density of states, making the precise location of the resonant levels ambiguous and thus making the comparison with spectroscopic experiments difficult. In the present work, we perform electronic-structure calculations for alkali-metal adlayers on the semi-infinite jellium surfaces to refine the results in I. Although the calculational method is quite different, this work corresponds to an extension to the finite-Θ regime of the well-known work of Lang and Williams,[25,26] and Hjelmberg *et al.*[27] on single-atom chemisorption on the semi-infinite jellium. (Short papers on part of the present work have been published).[28,29] The jellium model is not in particular meant to describe transition-metal substrates with localized d bands. Nevertheless, for properties such as the work-function change which depends on the charge distribution only in an averaged way, there is no qualitative difference between simple-metal and transition-metal substrates. The jellium substrate may be therefore useful for understanding the essence of properties which are insensitive to the exact nature of the substrate.

Currently, there is some debate on a few basic problems on alkali-metal adsorption on metals and semiconductors.[30-32] One is whether the adatom is neutral or positively charged, and another is whether the A-S bonding is covalent or ionic. As for the first question, part of

the controversy seems to stem from the lack of rigorous definitions for quantities such as ionicity and charge transfer. As for the second one, we point out that the covalent and ionic bondings are not completely contradictive concepts; the ionic bond is a limit of the strongly polarized covalent bond, and the bonding nature should change continuously as a function of the difference in electronegativity between the adatom and substrate. It may be said that the recent first-principles calculations exemplified significance of the covalency in the A-S bond which had been ignored in the Gurney model.

The outline of the present paper is as follows. In Sec. II we review shortly theoretical models of the alkali-metal adsorption proposed so far. In Sec. III the adlayer model in the present calculation and details of the calculational method are described. Section IV is the main part of the present paper which contains the results and discussion of the present calculation. Finally, summary is given in Sec. V. We use the Hartree atomic units with $m=e=\hbar=1$ throughout. The units of the energy and length are 27.2 eV and 0.529 Å, respectively.

II. IONIC AND COVALENT MODELS

The work-function decrease due to the alkali-metal adsorption, $\Delta\Phi(\Theta)$, is given as $\Delta\Phi(\Theta)=4\pi\Theta d(\Theta)/A$, where $d(\Theta)$ is the electric dipole moment induced on an adatom site due to the charge redistribution and A is the area of the unit cell at $\Theta=1$. The appearance of a maximum in $\Delta\Phi(\Theta)$ near half the monolayer coverage[1-3] originates from a rapid decrease of $d(\Theta)$ with increasing Θ.

The first model to explain this behavior was given by Gurney.[19] It is summarized as follows. The interaction between the adatom and substrate orbitals due to their direct overlap is weak, and its main effect is to broaden discrete levels of an isolated alkali-metal atom into rather sharp resonances. Because of the image shift,[33] the center of the valence s resonance is located above the Fermi level (E_F), and the s electron is mostly lost to the substrate. Consequently, the adatom is strongly ionized at low Θ. To keep the charge neutrality, screening charge is induced in the metal side, which leads to the dipole moment given as

$$d_1(\Theta)=D\left[1-\sum_{\alpha}\langle C_{\alpha}^{\dagger}C_{\alpha}\rangle\right], \tag{1}$$

where α denotes the adatom state, and D is the distance between the adatom nucleus and the image plane of the substrate. The rapid decrease of $d(\Theta)$ at higher Θ is attributed to the downward shift of the s resonance due to the dipole field from surrounding adatoms (depolarization field), which makes the adatom under consideration more neutral and therefore reduces $d_1(\Theta)$.

According to Eq. (1), $d_1(\Theta)$ is very sensitive to D. Lang and Williams[25] studied $d(\Theta)$ of Na, Si and Cl on the jellium with $r_s=2$ as a function of the jellium-adatom distance. In their calculation, $d(\Theta)$ for Cl with the localized valence orbitals was indeed small when the adatom is put on the image plane of the substrate ($D=0$), whereas $d(\Theta)$ for Na at $D=0$ was about 60% of that at the equilibrium Na-jellium distance.[34] This means either that Eq. (1) is not good as the expression of the ionic part of the dipole moment for Na with the extended $3s$ state especially when D is small, or that the dipole moment of another physical origin such as discussed in the below contributes appreciably to $d(\Theta)$.

To take account of the large polarizability of an isolated alkali-metal atom, Muscat and Newns[35] added the *intra-atomic* polarization term,

$$d_2(\Theta)=\sum_{\alpha,\alpha'}\lambda_{\alpha\alpha'}\langle C_{\alpha}^{\dagger}C_{\alpha'}\rangle+\text{c.c.}\ , \tag{2}$$

to the expression of $d(\Theta)$ in their model calculation based on the Anderson Hamiltonian. (They considered the mixing of the valence s and p_z states.) The dipole field from surrounding adatoms induces $d_2(\Theta)$ in the opposite direction to $d_1(\Theta)$, which accelerates the rapid decrease of $d(\Theta)$ at higher Θ.

It was explicitly shown in I that $d(\Theta)$ should also include the *interatomic* polarization term,[36]

$$d_3(\Theta)=\sum_{\alpha,\beta}\mu_{\alpha\beta}\langle C_{\alpha}^{\dagger}C_{\beta}\rangle+\text{c.c.}\ , \tag{3}$$

where β denotes the substrate state and $\mu_{\alpha\beta}$ is the dipole matrix element. This term reflects the covalency in the A-S bonding, i.e.,

$$E_c=\sum_{\alpha,\beta}V_{\alpha\beta}\langle C_{\alpha}^{\dagger}C_{\beta}\rangle+\text{c.c.}\ ,$$

where $V_{\alpha\beta}$ is the off-diagonal matrix element of the Hamiltonian. It was ignored in the previous model calculation based on the ionic adsorption picture. Its origin is the polarization of one-electron wave functions on the adatom site toward the interface (vacuum) side which is characteristic to the bonding (antibonding) state with respect to the A-S bonding. In case of the alkali-metal adsorption, the hybridization between the alkali-metal valence s orbital and the substrate orbital, whose tail has the p_z component when expanded on the adatom site, can induce a charge redistribution from the vacuum to the interface side of the adatom. Equation (3) takes a maximum value when the bonding-antibonding (B-A) boundary regarding the A-S bonding coincides with E_F, i.e., when the covalency E_c becomes the largest.

For a symmetric s resonance whose center coincides with the B-A boundary, $d_3(\Theta)$ becomes the largest when the resonance is half filled, i.e., when the adatom is neutral. Therefore $d_1(\Theta)$ and $d_3(\Theta)$ show very different behaviors as a function of the location of the resonance center relative to E_F (see Fig. 2 in I). The covalency in such a simple resonance takes a maximum value when there is no ionicity. As another example, we consider here the two-level system shown in Fig. 1. We assume that both the α and β sites have one electron when they are separated. The wave functions of the bonding and antibonding states are written as $\phi_b=C_1\phi_\alpha+C_2\phi_B$ and $\phi_a=C_2\phi_\alpha-C_1\phi_\beta$, respectively. ($C_1^2+C_2^2=1$ and $C_2>C_1$ if $\varepsilon_\alpha>\varepsilon_\beta$.) If the occupation numbers of ϕ_b and ϕ_a are n_b and n_a ($n_b+n_a=2$), we have

$$d_1=D(C_2^2-C_1^2)(n_b-n_a)/2$$

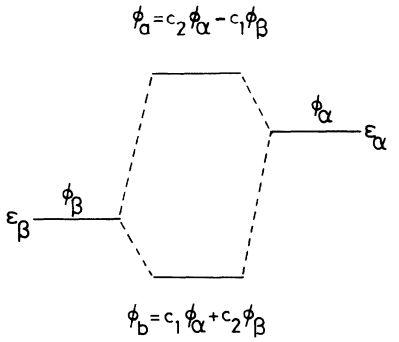

FIG. 1. Level scheme for the two-level system made of α and β sites with different site energies, ε_α and ε_β.

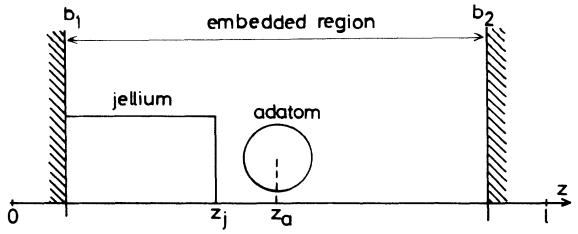

FIG. 2. Alkali-metal adlayer on the semi-infinite jellium surface. Only the embedded region with $b_1 \le z \le b_2$ is treated explicitly in the self-consistent calculation.

and

$$d_3 = 2\mu_{\alpha\beta} C_1 C_2 (n_b - n_a) .$$

Hence, $d_1(\Theta)$ and $d_3(\Theta)$ are proportional to each other in this case; both terms becomes the largest when ϕ_b are fully occupied, and the filling of the antibonding state ϕ_a decreases the ionicity and covalency of the molecule simultaneously.

In case of the Cs adsorption, Wimmer *et al.*[20,21] showed that the counter polarization of the Cs $5p$ core orbital also contributes to $d(\Theta)$. The effect may become smaller for lighter alkali-metal atoms with deeper core levels.

III. MODEL AND CALCULATIONAL METHOD

Our model is an extension of the work of Lang and Williams,[25,26] and Hjelmberg *et al.*[27] on the single-atom adsorption on jellium to finite coverages. We calculate the electronic structure of alkali-metal adlayers on semi-infinite jellium surfaces by a first-principles method within the local-density-functional approach. The method is a fully three-dimensional one which introduces no approximation such as taking the average of the potential energy in the planar direction,[37] and the presence of the semi-infinite substrate and the vacuum is taken into account by using the embedding method of Inglesfield.[38–40] Figure 2 shows the calculational geometry. Only the embedded region with $b_1 \le z \le b_2$ is explicitly treated, and the effects of the bulk jellium ($z < b_1$) and vacuum ($z > b_2$) are expressed in terms of complex embedding potentials acting on the two embedding surfaces at $z = b_1$ and $z = b_2$.

To describe one-electron wave functions and their logarithmic derivatives at the embedding surfaces, the Green function

$$G(\mathbf{r},\mathbf{r}',\varepsilon,\mathbf{k},\Theta) = \langle \mathbf{r} | [\varepsilon + i\delta - H(\mathbf{k},\Theta)]^{-1} | \mathbf{r}' \rangle$$

is expanded in terms of the nonorthogonal basis set

$$\phi_{\mathbf{k}+\mathbf{G},n}(\mathbf{r}) = \sqrt{2/Sl}\, \exp[i(\mathbf{k}+\mathbf{G})\cdot\mathbf{x}] \sin(k_n z) , \quad b_1 \le z \le b_2 \qquad (4)$$

where $k_n = n\pi/l$ ($n \ge 1$), S is the surface area, and $\mathbf{k}$ and $\mathbf{G}$ denote the two-dimensional wave vector and reciprocal-lattice vector, respectively. Corresponding to Eq. (4), the electron charge density is expanded in the form,

$$n(\mathbf{r},\Theta) = \sum_G \sum_{m \ge 0} n(\mathbf{G},m) \exp(i\mathbf{G}\cdot\mathbf{x}) \cos(k_m z) , \quad b_1 \le z \le b_2 . \qquad (5)$$

Given an input charge density, the Hartree potential for a nonzero $\mathbf{G}$ component is calculated directly as

$$V_H(\mathbf{G},z) = \frac{2\pi}{|\mathbf{G}|} \int_{b_1}^{b_2} dz' \exp(-|\mathbf{G}|\,|z-z'|) n_t(\mathbf{G},z') , \qquad (6)$$

where

$$n_t(\mathbf{G},z) = \sum_{m \ge 0} [\, n(\mathbf{G},m) + n_a(\mathbf{G},m) + n_j(\mathbf{G},m)] \cos(k_m z) . \qquad (7)$$

In Eq. (7), $n_a(\mathbf{G},m)$ and $n_j(\mathbf{G},m)$ are the coefficients of the core charge density of adatoms and the background positive charge of the jellium expanded in the same form as Eq. (5), respectively,[41] We use the norm-conserving pseudopotential for alkali-metal ion cores.[42] In this case, $n_a(\mathbf{G},m)$ represents the local part of the pseudopotential. Equation (6) leads to

$$V_H(\mathbf{G},z) = \sum_{m \ge 0} \frac{4\pi n_t(\mathbf{G},m)}{|\mathbf{G}|^2 + k_m^2} \cos(k_m z) - \sum_{m \ge 0} \frac{2\pi n_t(\mathbf{G},m)}{|\mathbf{G}|^2 + k_m^2} \left[\exp[-|\mathbf{G}|(z-b_1)] \left[\cos(k_n b_1) + \frac{k_n}{|\mathbf{G}|} \sin(k_n b_1) \right] + \exp[-|\mathbf{G}|(b_2 - z)] \left[\cos(k_n b_2) - \frac{k_n}{|\mathbf{G}|} \sin(k_n b_2) \right] \right] . \qquad (8)$$

The latter two contributions are actually two or three orders of magnitude smaller than the first one, and are not important.

The calculation of the Hartree potential for $\mathbf{G}=0$ needs special care. It cannot be evaluated simply as the first term of Eq. (8) because this term includes the electric field due to the unphysical charge densities in the regions, $0\le z\le b_1$ and $b_2\le z\le l$. To remove the electric field from the former region, we add

$$c_1 n_1(z)=c_1\sum_m n_1(m)\cos(k_m z) \tag{9}$$

to $n_t(\mathbf{G}=0,z)$, where $n_1(z)$ is a model charge density localized in the interval $[0,b_1]$ and normalized to unity. c_1 is determined through the constraint that the total charge within the region $0\le z\le b_1$, vanishes, which leads to the equation

$$c_1=-\int_0^{b_1} dz\, n_t(\mathbf{G}=0,z)\ . \tag{10}$$

The final potential energy does not depend on the choice of $n_1(z)$ as far as sufficiently large m values are kept in the expansion equation (9). In the actual calculation, $2\sin^2(\pi z/b_1)/b_1$ is used as $n_1(z)$. In the same way, a localized model charge density $c_2 n_2(z)$ is added to $n_t(\mathbf{G}=0,z)$ to neutralize the region $b_2\le z\le l$. We use $2\sin^2[\pi(l-z)/(l-b_2)]/(l-b_2)$ as $n_2(z)$.

Since the embedding calculation for a fixed E_F assumes no charge neutrality of the system, the embedded region $b_1\le z\le b_2$ becomes positively or negatively charged unless the charge density is calculated with the self-consistent input potential. There should be a net charge in the jellium side which exactly cancels the excess charge in the embedded region. The dipole layer formed by these excess charge densities in the embedded region and in the jellium side works as a restoring force toward the charge neutrality in the next iteration. To take account of this effect, we also add $q_1 n_1(z)$ to $n_t(\mathbf{G}=0,z)$ where q_1 is determined by

$$q_1=-\int_{b_1}^{b_2} dz\, n_t(\mathbf{G}=0,z)\ . \tag{11}$$

The Hartree potential for $\mathbf{G}=0$ is then calculated as

$$V_H(\mathbf{G}=0,z)=\sum_{m\ge 1}\frac{4\pi}{k_m^2}[\,n_t(\mathbf{G}=0,m)+(c_1+q_1)n_1(m)+c_2 n_2(m)]\cos(k_m z)+V_0\ , \tag{12}$$

where V_0 is adjusted so that the total potential energy becomes continuous at $z=b_1$. After the convergence, the charge neutrality in the embedded region is conserved up to the order of 10^{-3} or 10^{-4} of the total positive charge in the embedded region.

The exchange-correlation potential is expanded in the same form as Eq. (5). The expansion coefficients are determined by evaluating the potential energy at sampling mesh points in the unit cell and taking the Fourier transform. The matrix elements of the Hartree and exchange-correlation potentials are then calculated analytically. The matrix element of the kinetic-energy operator is given as

$$H_{\rm kin}(\mathbf{G},n;\mathbf{G}',n')=\frac{(\mathbf{k}+\mathbf{G})^2}{l}\int_{b_1}^{b_2} dz\,\sin(k_n z)\sin(k_{n'}z)\delta_{\mathbf{G},\mathbf{G}'}+\frac{k_n k_{n'}}{l}\int_{b_1}^{b_2} dz\,\cos(k_n z)\cos(k_{n'}z)\delta_{\mathbf{G},\mathbf{G}'}\ . \tag{13}$$

Since the potential energy is constant in the bulk jellium ($z\le b_1$) and in the vacuum ($z\ge b_2$), the z part of the one-electron wave function for a given $(\mathbf{k}+\mathbf{G},\varepsilon)$ is given by $\exp(-ik_z z)$ with $k_z=[2\varepsilon-(\mathbf{K}+\mathbf{G})^2]^{1/2}$ for $z\le b_1$, and by $\exp(ik_z' z)$ with $k_z'=[2(\varepsilon-\varepsilon_{\rm vac})-(\mathbf{K}+\mathbf{G})^2]^{1/2}$ for $z\ge b_2$. Here the one-electron energy ε is measured from the bottom of the jellium potential, and $\varepsilon_{\rm vac}$ is the potential barrier at $z=b_2$ which is determined self-consistently. The matrix elements of the energy-dependent embedding potentials at $z=b_1$ and $z=b_2$ are obtained from the logarithmic derivatives of these wave functions at the embedding surfaces. They are given as

$$H_{b_1}(\mathbf{G},n;\mathbf{G}',n')=\frac{[(\mathbf{k}+\mathbf{G})^2-2\varepsilon]^{1/2}}{l}\times\sin(k_n b_1)\sin(k_{n'}b_1)\delta_{\mathbf{G},\mathbf{G}'}\ , \tag{14}$$

and

$$H_{b_2}(\mathbf{G},n;\mathbf{G}',n')=\frac{[(\mathbf{k}+\mathbf{G})^2-2(\varepsilon-\varepsilon_{\rm vac})]^{1/2}}{l}\times\sin(k_n b_2)\sin(k_{n'}b_2)\delta_{\mathbf{G},\mathbf{G}'}\ , \tag{15}$$

where the imaginary part of H_{b_1} and H_{b_2} is chosen negative.[43] The Green function is obtained by the inversion of $\varepsilon\bar{S}-\bar{H}$, where $\bar{H}$ and $\bar{S}$ denote the Hamiltonian and overlap matrices, respectively. The output charge density is calculated from the Green function as

$$n(\mathbf{r},\Theta)=-\frac{1}{\pi}\int\frac{2d\mathbf{k}}{(2\pi)^2}\int_0^{E_F} d\varepsilon\,{\rm Im}G(\mathbf{r},\mathbf{r},\varepsilon,\mathbf{k},\Theta)\ , \tag{16}$$

where the $\mathbf{k}$ integration is performed in the surface Brillouin zone, and the prefactor 2 accounts for spin degeneracy.

We use the higher-dimensional Anderson method reformulated in the language of the quasi-Newton method by Blügel[44] for the mixing procedure toward self-consistency. In this method, the input and output charge densities in all the previous iterations are used to generate the input charge for the next iteration. The iteration procedure is continued until the difference between the input and output surface dipole layers becomes less than 10^{-5} a.u. In the actual calculation, the embedding parameters, b_1, z_j, b_2, and l are set equal to 2, 10, 24, and 26 a.u., respectively. With these values, the electron density near $z=b_2$ is of the order of 10^{-7} a.u., which is sufficient for the convergence of the surface dipole layer. Also the thickness of the embedded jellium slab, $z_j-b_1=8$ a.u. is sufficient for the convergence of the bulk electron density because of the efficient metallic screening. The cut-off energy for the basis-set equation (4) is chosen as 5 Ry, which leads to ~ 1250 basis functions for the lowest Θ in the present calculation. This cut-off value is large enough for Na for which we show results in the next section.

However, higher cutoff energies may be necessary for heavier alkalimetals (K, Rb, and Cs) in order to describe their low-lying valence d states. The cut-off energy for the potential energy is 20 Ry for nonzero $\mathbf{G}$ components, whereas it is chosen as 324 Ry for $\mathbf{G}=0$. Such a large value is necessary for $\mathbf{G}=0$ to make the expansion equation (9) well converged.

IV. RESULTS AND DISCUSSION

In the present paper we show results for hexagonal Na adlayers. Although the adlayers were assumed to form square lattices in I, there is no qualitative difference in electronic properties between the hexagonal and square adlayers because alkali-metal atoms have only extended valence s electrons. In I, the jellium with $r_s=2.1$ was used to simulate a high-density metal substrate. To examine to which extent the results in I are general, we study here three jellium substrates with $r_s=2$, 3, and 4, whose positive background density is roughly equal to the free-electron density of Al, Ag, and Na. The work function of these jellium surfaces are 3.9, 3.5, and 3.0 eV for $r_s=2$, 3, and 4, respectively. Given a nearest-neighbor Na-Na distance $a_{\parallel}$, the only one free-parameter is the distance between the Na nucleus and the edge of the background density of the jellium D_{as}. The total-energy calculation at $a_{\parallel}=9.35$ a.u. gave $D_{as}=3.1$, 2.7, and 2.5 a.u. as the equilibrium Na-jellium distance for $r_s=2$, 3, and 4, respectively.[45] It was shown in I that the adlayer shows a small outward relaxation with increasing Θ because of the weakening of the A-S bonding. However, as the magnitude of this relaxation is much smaller than the orbital size of Na 3s, the electronic structure of the adlayer changes only rather little within this relaxation range. To save the computational work, the same D_{as} values as for $a_{\parallel}=9.35$ a.u. are used for the other coverages.

A. Charge density and work function

Figure 3 shows contour maps of the charge density $n(\mathbf{r},\Theta)$ for several Na adlayers on the jellium with $r_s=2$ on the vertical-cut plane containing nearest-neighbor Na atoms. The positions of the jellium edge and Na nuclei are indicated by an arrow and solid circles, respectively. In the planar direction, the charge density varies appreciably with Θ: The outermost density contours at $a_{\parallel}=7$ a.u. are mostly parallel to the surface, reflecting the metallic nature of the adlayer, whereas the corresponding ones at $a_{\parallel}=17$ a.u. near Na nuclei are highly corrugated and atomiclike. Perpendicular to the surface, the Na valence charge, which acts as electron cloud that screens the positive ion cores, is slightly polarized toward the metal side of the adlayer regardless of Θ.

To see this effect more clearly, we calculate the difference charge $\delta n(\mathbf{r},\Theta)$ defined as the charge density of the Na-covered jellium surface minus the superposed density of the clean jellium surface and the isolated Na layer. The work-function change $\Delta\Phi(\Theta)$ is related with $\delta n(\mathbf{r},\Theta)$ by $\Delta\Phi(\Theta)=4\pi\int d\mathbf{r}\, z\,\delta n(\mathbf{r},\Theta)/S$. Figures

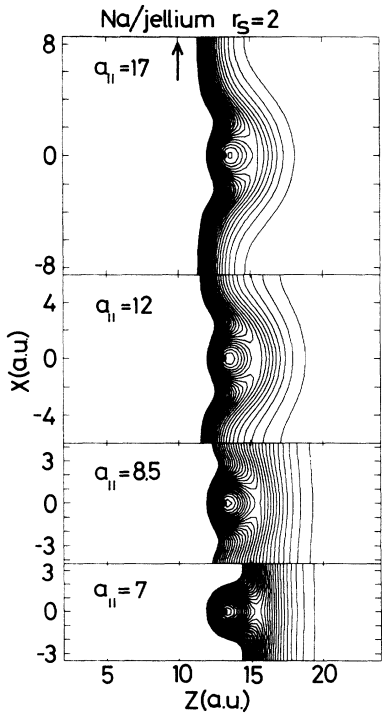

FIG. 3. Contour maps of the charge density $n(\mathbf{r},\Theta)$ for hexagonal Na adlayers on the semi-infinite jellium with $r_s=2$ in a plane normal to the surface containing nearest-neighboring Na atoms. The contour spacing is 1.2×10^{-4} a.u. The solid circles and arrow indicate that the Na core and edge of the jellium substrate, respectively.

4(a)–4(c) show contour maps of the calculated $\delta n(\mathbf{r},\Theta)$ for several Na adlayers on the three-jellium substrates. Here the solid and dashed contours correspond to positive and negative values of $\delta n(\mathbf{r},\Theta)$, and the contour spacings are 5×10^{-4} and 2.5×10^{-4} a.u. for solid and dashed contours, respectively. The contour map at the lowest Θ for $r_s=2$ is very similar to that given by Lang and Williams[25] for the single Li atom on the same substrate, which implies the direct Na-Na interaction is very small at this Θ. The polarization arrangement of the Na valence charge toward the metal side is seen in Fig. 4 as the increase and decrease of charge in the interface and vacuum side of Na, respectively. The charge depletion area also appears in the jellium side. It becomes more extended into the bulk with increasing r_s, since the electron gas with lower density has a larger screening length. The charge buildup in the interface and the depletion in both sides of the interface indicates formation of the Na-jellium bond. For a fixed Θ, $\delta n(\mathbf{r},\Theta)$ for the three r_s values are similar with one another, except that the amplitude of $\delta n(\mathbf{r},\Theta)$ is enhanced with decreasing r_s. As a result, the adatom dipole moment $d(\Theta)$ at a fixed Θ becomes larger for the jellium substrate with smaller r_s (larger work function). For a fixed r_s, the polarization arrangement of the Na valence charge is seen to become weaker with increasing Θ: The amplitude of the charge depletion in the vacuum side of Na becomes smaller, and at the same time, its centroid shifts toward the Na plane.

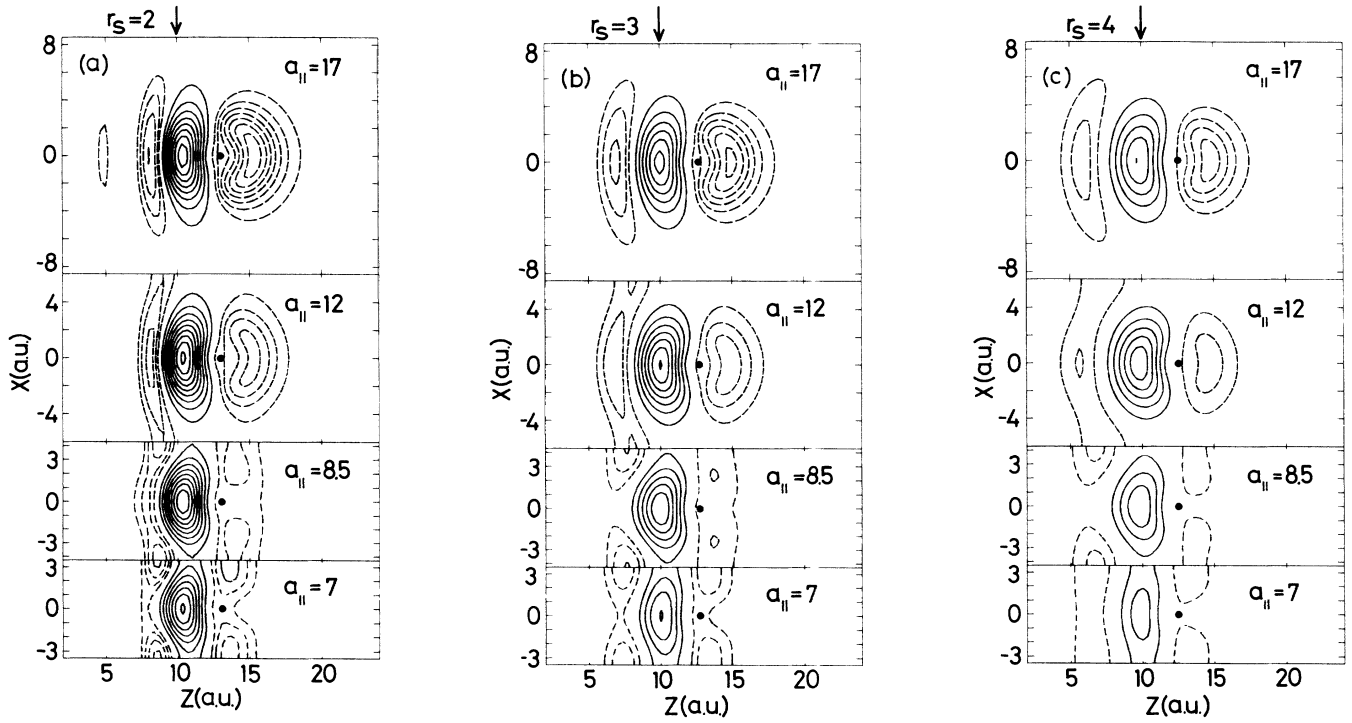

FIG. 4. Contour maps of the difference charge $\delta n(\mathbf{r},\Theta)$ for hexagonal Na adlayers on the semi-infinite jellium with (a) $r_s=2$, (b) $r_s=3$, and (c) $r_s=4$ on the same vertical-cut planes as in Fig. 3. The solid and dashed contours correspond to positive and negative values of $\delta n(\mathbf{r},\Theta)$, and the contour spacings are 5×10^{-4} a.u. and 2.5×10^{-4} a.u., respectively.

These behaviors result in a rapid decrease of $d(\Theta)$ with increasing Θ.

The calculated work function $\Phi(\Theta)$ and $d(\Theta)$ are shown in Fig. 5 as a function of Θ for the three jellium substrates. Here, just for the sake of convenience, the Na coverage is measured relative to the coverage corresponding to $a_{\|}=8.5$ a.u. (Θ_m). The work-function curves reproduce the observed well-known behavior, i.e., a rapid decrease at lower Θ, which is followed by a minimum and a subsequent weaker rise toward saturation values. It is interesting that $\Phi(\Theta)$ at the highest Θ depends very little on the substrate, although there is ~1 eV difference in $\Phi(\Theta)$ at $\Theta=0$ among the three curves. It may be said that the effect of the substrate is screened out by the adlayer when the surface is mostly covered by adatoms.

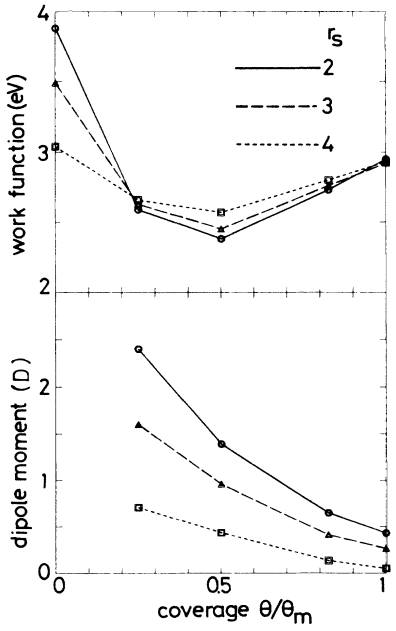

FIG. 5. Calculated work-function $\Phi(\Theta)$ and adatom dipole moment $d(\Theta)$ for the hexagonal Na adlayers on three jellium surfaces.

B. Adatom density of states

The structure of the Na-induced resonant levels was not surveyed into very details in I because of the slab approximation for the substrate. The ambiguity is lifted in the present semi-infinite calculation. We study the adatom density of states (DOS) defined by

$$\rho_a(\varepsilon,\Theta)=-\frac{1}{\pi}\int\frac{2d\mathbf{k}}{(2\pi)^2}\int_R d\mathbf{r}[\,\mathrm{Im}G(\mathbf{r},\mathbf{r},\varepsilon,\mathbf{k},\Theta)-\mathrm{Im}G(\mathbf{r},\mathbf{r},\varepsilon,\mathbf{k},\Theta=0)]\,, \tag{17}$$

where the volume integration is performed in the Na atomic sphere with radius R.[46] Qualitative features of $\rho_a(\varepsilon,\Theta)$ are insensitive to the small difference in R, and we use $R=3.5$ a.u. The solid curves in Figs. 6(a)–6(c) are $\rho_a(\varepsilon,\Theta)$ of Na on the three jellium substrates. The dashed, dotted-dashed, and dotted curves show the decomposition of $\rho_a(\varepsilon,\theta)$ into the s, $p_{\|}(p_x+p_y)$, and p_z partial DOS, respectively. The calculated $\rho_a(\varepsilon,\Theta)$ at

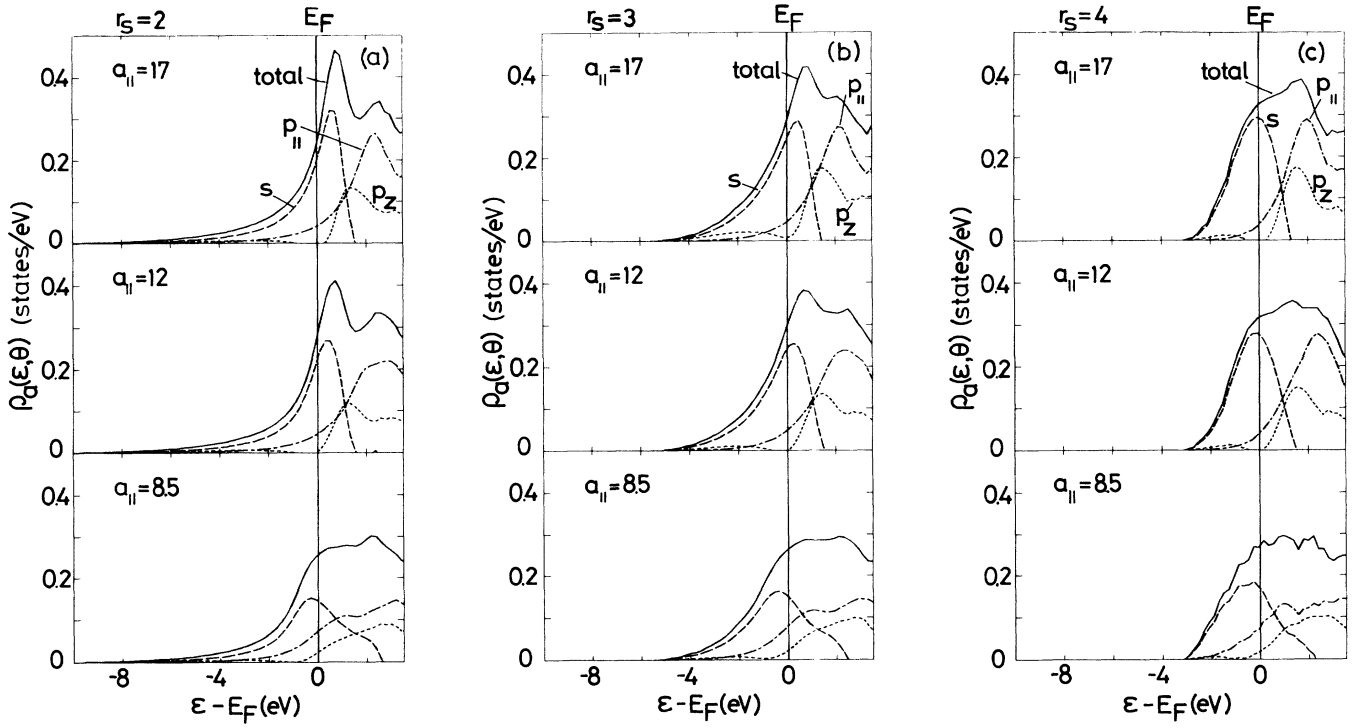

FIG. 6. Adatom density of states $\rho_a(\varepsilon,\Theta)$ for hexagonal Na adlayers on the jellium surface with (a) $r_s=2$, (b) $r_s=3$, and (c) $r_s=4$ (solid curves). The dashed, dotted-dashed, and dotted curves show the decomposition of $\rho_a(\varepsilon,\Theta)$ into the s, $p_\parallel(p_x+p_y)$, and p_z partial density of states, respectively.

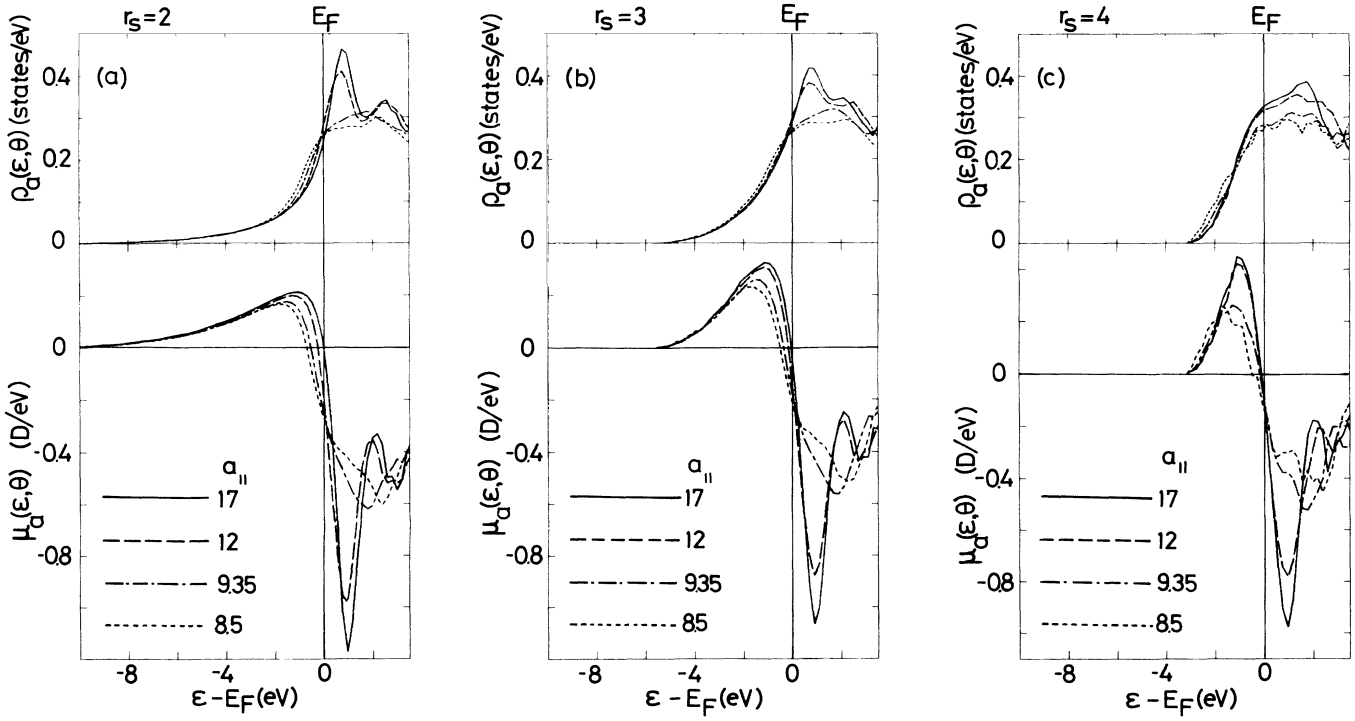

FIG. 7. Upper panels: Adatom density of states $\rho_a(\varepsilon,\Theta)$ for hexagonal Na adlayers on the semi-infinite jellium with (a) $r_s=2$, (b) $r_s=3$, and (c) $r_s=4$. Lower panels: Corresponding dipole density of states $\mu_a(\varepsilon,\Theta)$ for the Na adlayers.

$a_{\parallel}=17$ a.u. on the jellium with $r_s=2$ is very similar to that given by Lang and Williams[26] in the low-Θ limit.

First, we discuss behaviors at low coverages. For $r_s=2$ and 3, the calculated $\rho_a(\varepsilon,\Theta)$ has two atomiclike peaks above E_F, whereas they are not well separated for $r_s=4$. The lower peak corresponds to a hybridized state of Na $3s$ and $3p_z$. The two components do not form separated peaks because of the strong A-S interaction. It will be shown later that this resonance is an antibonding state with regard to the A-S bonding whose wave function is strongly polarized toward the vacuum side of Na. On the other hand, the second peak is mainly due to Na $3p_{\parallel}$. With increasing r_s, the peak positions of the s- and $p_{\parallel}$-DOS shift gradually to lower energies, whereas that of the p_z DOS remains nearly unchanged. At $r_s=4$, which corresponds to the adsorption of Na on Na, the s DOS is fairly symmetric with respect to E_F, and the energy difference between the $p_{\parallel}$ and p_z DOS is not so large as those for $r_s=2$ and 3.

Next, we discuss the Θ dependence of the adatom DOS. For a fixed r_s, the calculated $\rho_a(\varepsilon,\Theta)$ shows only minor changes roughly up to the coverage of the work-function minimum ($a_{\parallel}=12$ a.u.) in spite of the large lowering of the electrostatic potential in the vacuum. The peak position of the s-p_z hybridized state shifts a little downward with increasing Θ, since its wave function is strongly polarized toward the vacuum and therefore can feel the potential lowering in the vacuum.[47] On the other hand, larger changes in $\rho_a(\varepsilon,\Theta)$ occur for coverages higher than the work-function minimum: The atomiclike peaks in $\rho_a(\varepsilon,\Theta)$ at low Θ disappear rapidly, corresponding to the formation of broad adlayer bands due to the large orbital overlap among nearby Na atoms. The upper panels of Fig. 7(a)–7(c) summarize the Θ dependence of $\rho_a(\varepsilon,\Theta)$ for Na adlayers on the three jellium substrates. As compared with the rapid decrease of $d(\Theta)$ with increasing Θ, the occupied part of $\rho_a(\varepsilon,\Theta)$ is remarkably insensitive to Θ. This means that the adatom dipole moment is caused mostly by the charge redistribution within the Na atomic sphere and that the charge flow to the region outside the sphere is very small. Therefore if the Na charge state $n_a(\Theta)$ is evaluated simply as the area of the occupied part of $\rho_a(\varepsilon,\Theta)$, it is quite insensitive to Θ. Of course, the Friedel sum rule ensures $n_a(\Theta)=1$ if the volume integration in Eq. (17) is performed in the entire unit cell. Thus we need examine $n_a(\Theta)$ as a function of R. Figure 8 shows $n_a(\Theta)$ of Na on the three jellium substrates for several R values. They are compared with the number of electrons in the same sphere calculated for the isolated (neutral) Na layers, $n_{\rm iso}(\Theta)$ (dotted lines). Both $n_a(\Theta)$ and $n_{\rm iso}(\Theta)$ increase rapidly at very high Θ because of the significant orbital overlap among nearby adatoms. Despite the appreciable difference in $\rho_a(\varepsilon,\Theta)$ among the three substrates, the calculated $n_a(\Theta)$ for the three substrates can be seen very close to one another. They are a little larger than $n_{\rm iso}(\Theta)$ for $R\geq 3$ a.u. in some intermediate coverages. More importantly, they are remarkably close to $n_{\rm iso}(\Theta)$ even for such a small R value as $R=2$ a.u. where the sphere contains only less than 0.1 valence electrons. In this sense, it

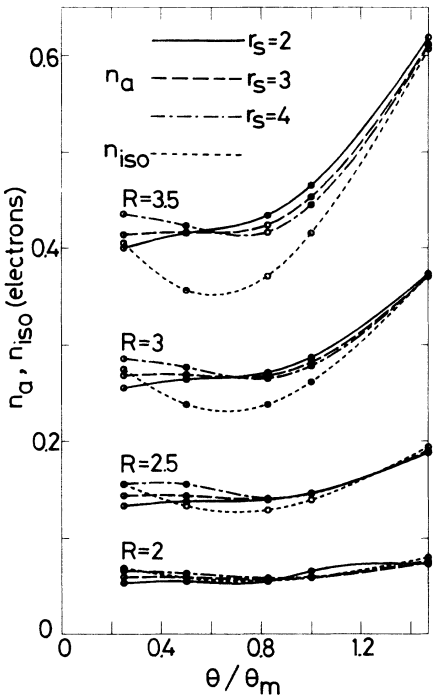

FIG. 8. Na charge state $n_a(\Theta)$ defined by the area of the occupied part of $\rho_a(\varepsilon,\Theta)$ for several values of the sphere radius R. The dotted lines show $n_{\rm iso}(\Theta)$ calculated for isolated Na layers.

is not appropriate to claim that the Na atom is positively charged. This result is in consistent with the recent core-level measurement of Riffe, Wertheim, and Citrin[23] for the W(110) substrate where the core-level shift of the surface W atoms due to Na, K, and Cs was found negligibly small as compared with that caused by O.

In Fig. 9 we plot the s part of the total potential expanded at a Na site which gives the site energy of s orbitals in the LCAO (linear combination of atom orbitals) approach. It is seen the total s potential is very insensitive to Θ within the Na atomic sphere in spite of the large lowering of the electrostatic potential in the vacuum. Physically, this implies that the Na atom is actually adsorbed at a position where the screening of the metallic substrate still works so efficiently that it feels the potential lowering in the vacuum very little. In fact, around the potential minimum ($R\sim 2.2$ a.u.), the s potential takes the lowest value at $a_{\parallel}=17$ a.u. although the potential lowering in the vacuum becomes the largest at $a_{\parallel}=12$ a.u.[47] The Θ-independent s potential in Fig. 9 is in accord with the absence of a large change in $n_a(\Theta)$ with increasing Θ.

It might be claimed that part of the charge in a Na sphere should be attributed to the image charge. Indeed, in first-principles calculations where adatom and substrate orbitals such as used in model analyses based on the Anderson Hamiltonian[35,49,50] cannot be uniquely defined, it is impossible to divide the calculated $\rho_a(\varepsilon,\Theta)$ into the screening charge of the substrate and the true Na valence state in a unique way. (This is especially the case for alkali-metal atoms which have very extended valence

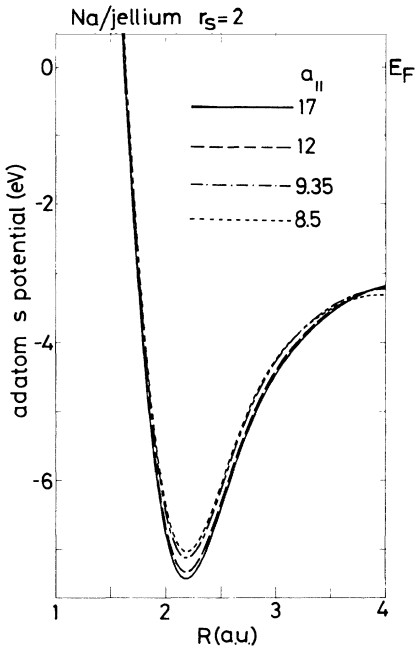

FIG. 9. s part of the total adatom potential for a Na atom on the semi-infinite jellium with $r_s=2$. R denotes the distance from the Na nucleus, and the potential energy is measured from E_F.

orbitals that significantly overlap with substrate orbitals.) Moreover, these two components cannot be separated even in any experiments such as photoemission, metastable-He* deexcitation, and core-level shift. Therefore it may not be very fruitful to try to determine the exact value of the ionicity or charge transfer, as far as we do not have rigorous definitions for these quantities. The present result that $n_a(\Theta)$ is very close to $n_{\rm iso}(\Theta)$ even for small R and Θ may not necessarily signify that the Na charge state as defined in the Anderson-type model calculation is close to neutral. The chemical trend seen in $\rho_a(\varepsilon,\Theta)$ at low Θ, such that the peak position of the s-partial DOS shifts to higher energies relative to E_F with decreasing r_s, may indicate the increase of the ionic contribution to the A-S bonding for the substrate with the larger work function. Nevertheless, since the depolarization field at the Na site is very small, at least, it is sure that the rapid decrease of $d(\Theta)$ for the present system cannot be explained merely in terms of the adatom neutralization due to the dipole-dipole interaction.

C. Formation of adlayer bands

The disappearance of atomiclike resonances in $\rho_a(\varepsilon,\Theta)$ at higher Θ indicates formation of the broad adlayer bands. Recently, Horn *et al.*[51] succeeded for the first time in observing a partially occupied free-electron-like band for the ordered $(\sqrt{3}\times\sqrt{3})R30°$ K monolayer on Al(111).[52] On the theory side, some of previous slab calculations predicted the existence of such free-electron-like bands derived from the alkali-metal valence states.[20,53] However, slab calculations give no information on the width or shape of adatom resonances which is necessary for the comparison with experiments.

To examine the energy dispersion of the adlayer bands, we calculate

$$\rho_a(\mathbf{k},\varepsilon,\Theta)=-\frac{2}{\pi}\int_R dr\ \mathrm{Im}G(\mathbf{r},\mathbf{r},\varepsilon,\mathbf{k},\Theta)\ . \tag{18}$$

Here, for the better comparison with photoemission spectra, we do not subtract the density of states of the jellium substrate [second term of Eq. (17)] in the definition Eq. (18). The solid curves in Figs. 10(a) and 10(b) show $\rho_a(\mathbf{k},\varepsilon,\Theta)$ for the Na adlayer with $a_{\parallel}=9.35$ a.u. on the jellium with $r_s=2$ along the $\bar{\Gamma}$-$\bar{K}$ and $\bar{\Gamma}$-$\bar{M}$ lines in the surface Brillouin zone (SBZ), respectively. The lattice constant corresponds to that of the $(\sqrt{3}\times\sqrt{3})R30°$ monolayers on Al(111). $\rho_a(\mathbf{k},\varepsilon,\Theta)$ has much richer structures than $\rho_a(\varepsilon,\Theta)$ in Fig. 7. The lowest peak, contributed by s and also by the p_z state in its upper half, disperses upward with increasing $\mathbf{k}$, and crosses E_F around the middle of $\bar{\Gamma}$-$\bar{M}$ and $\bar{\Gamma}$-$\bar{K}$. Its dispersion below E_F is in good agreement with the experimental one of Horn *et al.*[51] In contrast to the case of the isolated Na monolayer, the p_z resonance is greatly broadened, and does not form a separated peak in $\rho_a(\mathbf{k},\varepsilon,\Theta)$. The $p_{\parallel}$-like peak is located 6.4 eV above E_F at $\bar{\Gamma}$. Its lowest branch disperses downward and nearly degenerates with the s-like band at $\bar{K}$ and $\bar{M}$. If the peak energies of $\rho_a(\mathbf{k},\varepsilon,\Theta)$ are plotted as a function of $\mathbf{k}$, one finds that the resultant band structure is very close to that of the two-dimensional free-electron gas folded in the hexagonal SBZ.[29] The formation of free-electron-like bands at higher Θ is not a very obvious fact because they originate from rather weak Na ion core potentials and are easily modified by stronger substrate potentials.[30,32] One interesting point is that the calculated band structure has very small energy splittings at zone boundaries; the s and $p_{\parallel}$ resonances are almost degenerate at $\bar{K}$ and $\bar{M}$, while the corresponding energy splitting for the isolated Na layer amounts to $\sim$0.5 eV.[54] This is not unexpected since the wave functions of the resonances are delocalized into the substrate and therefore feel the periodicity of the Na potentials less than those in the isolated layer. Here it may be worth commenting that for heavier alkali-metals (K, Rb, and Cs), the energy dispersion of the adlayer band structure may be modified from that of the free-electron gas, especially for the unoccupied part because of the low-lying alkali-metal valence d states.[29] For example, Chubb *et al.*[21] showed that the interaction between the Cs d and Mo d states induces a large Cs d component in the surface DOS near E_F, and consequently increases the d charge in the adlayer.

Figure 10(c) shows $\rho_a(\mathbf{k},\varepsilon,\Theta)$ at a lower Θ corresponding to the work-function minimum along $\bar{\Gamma}$-$\bar{K}$. Although $\rho_a(\varepsilon,\Theta)$ at this Θ in Fig. 6(a) still appears atomiclike, the s-band width along $\bar{\Gamma}$-$\bar{K}$ already amounts to 1.1 eV. The s-band width for the corresponding isolated Na layer is 0.95 eV, so that the transfer energy between the neighboring Na sites is a little enhanced as compared with that in the isolated layer owing to the indirect interaction intermediated by the substrate states.

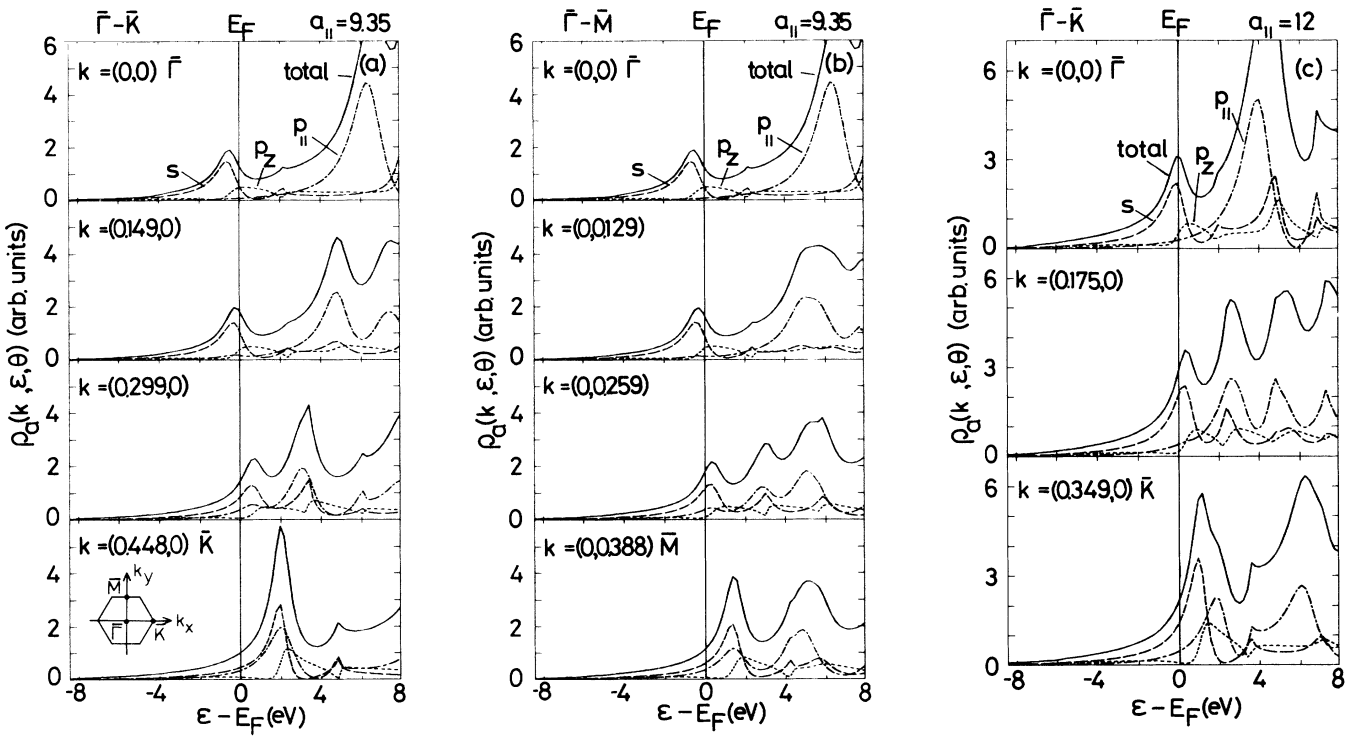

FIG. 10. $\rho_a(\mathbf{k},\varepsilon,\Theta)$ for the hexagonal Na adlayer with $a_{\parallel}=9.35$ a.u. on the jellium with $r_s=2$ along (a) $\bar{\Gamma}$-$\bar{K}$ and (b) $\bar{\Gamma}$-$\bar{M}$. (c) $\rho_a(\mathbf{k},\varepsilon,\Theta)$ for the hexagonal Na adlayer with $a_{\parallel}=12$ a.u. on the jellium with $r_s=2$ along $\bar{\Gamma}$-$\bar{K}$. Solid, dashed, dotted-dashed, and dotted curves correspond to the total s, $p_{\parallel}$, and p_z density of states, respectively.

Horn *et al.* also studied the normal photoemission spectra of K/Al(111) as a function of the K coverage. The spectra showed a quite different Θ dependence from that observed in the Penning experiment of Woratschek *et al.* for K/Cu(110).[55] The latter experiment suggested appreciable occupation of K 4*s* even in the lowest Θ, whereas the photoemission spectra showed a clear signal of K 4*s* only at higher Θ. A qualitative argument for this discrepancy was given by Horn *et al.*[51] in terms of the formation of adlayer bands and the different cross sections in the two experiments. Here we try to give a more quantitative explanation to resolve the different behaviors in the two experiments. Figure 11 shows $\rho_a(\mathbf{k},\varepsilon,\Theta)$ at $\mathbf{k}=0$ ($\bar{\Gamma}$) which may correspond to the normal emission spectra in photoemission for several Na adlayers on the jellium with $r_s=2$. There is a good agreement between the experimental data of Horn *et al.*[51] and Fig. 11 below E_F: For lower Θ, they show only a tail-like structure which is difficult to identify in experiments, whereas a distinct peak appears for higher Θ. However, this does not indicate the depolarization shift of the adatom state, but originates from the increase in the Na bandwidth with increasing Θ. On the other hand, in Penning experiments, because of the lack of the $\mathbf{k}$ conservation, the experimental spectra may be better compared with the total adatom DOS. Then the rather Θ-independent $\rho_a(\varepsilon,\Theta)$ in Fig. 7 is again in good agreement with the observation of

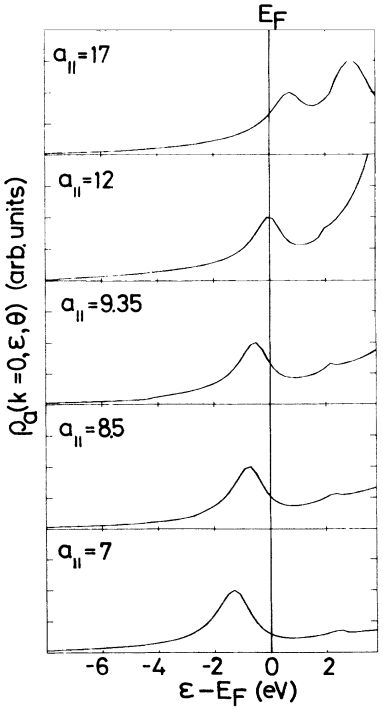

FIG. 11. $\rho_a(\mathbf{k},\varepsilon,\Theta)$ at $\mathbf{k}=0$ for several Na adlayer on the jellium with $r_s=2$.

Woratschek *et al.*[55] where the intensity of the K 4*s* resonance increased almost linearly with increasing Θ. To be accurate, the K 4*s* intensity was found to increase more than linearly at higher Θ in their experiment. However, this can be also understood as the matrix element effect, since the Na valence charge is less polarized toward the metal at higher Θ, and therefore has a larger orbital overlap with the incoming metastable He* atoms.

D. Dipole density of states

In order to examine the origin of $d(\Theta)$ as well as the nature of the Na-jellium bonding, we calculate the dipole DOS $\mu_a(\varepsilon,\Theta)$ which is defined in the same way as $\rho_a(\varepsilon,\Theta)$ except for an extra factor of $(z-z_a)$ in the volume integral of Eq. (17). The induced dipole moment within the sphere is obtained by integrating $\mu_a(\varepsilon,\Theta)$ up to E_F. It was found in I that $\mu_a(\varepsilon,\Theta)$ shows very similar ε dependence as another off-diagonal quantity, "bond-order" density. The calculated $\mu_a(\varepsilon,\Theta)$ for the three jellium substrates are shown in the lower panels of Fig. 7. The positive (negative) sign of $\mu_a(\varepsilon,\Theta)$ indicates polarization of the one-electron state toward the interface (vacuum) side of the adlayer, and thus the state can be regarded as a bonding (antibonding) state with respect to *A-S* bonding. It is seen that the atomiclike resonance at low Θ above 1 eV above E_F (the *s*-p_z hybridized state for $r_s=2$ and 3) is an antibonding state whose wave function is strongly polarized toward the vacuum side of Na atoms, as stated before. The occupied states are, on the other hand, polarized toward the interface, which thus leads to the bond charge in the interface shown in Fig. 4.

Despite the work-function difference of nearly 1 eV among the three jellium surfaces, the *B-A* boundary in $\mu_a(\varepsilon,\Theta)$ coincides well with E_F at the lowest Θ for all the substrates. Such a rapid change of the sign of $\mu_a(\varepsilon,\Theta)$ at E_F may not be expected for the substrates with $r_s=2$ and 3, as the corresponding $\rho_a(\varepsilon,\Theta)$ is smooth near E_F, showing no particular structure. The coincidence of the *B-A* boundary with E_F implies that the covalency in the *A-S* bonding (E_c) and the interatomic polarization term $d_3(\Theta)$ become the largest at the lowest Θ, independently of the kind of the substrate. In the classical model, the downward shift of the *s* resonance by the depolarization field was believed to increase E_c, and it was sometimes stated that the *A-S* bonding changes from ionic to covalent with increasing Θ. However, the above results show that a partial filling of the unoccupied part of the resonance, if any, via the indirect or direct Na-Na interaction actually decreases E_c, since it corresponds to the strong antibonding state. The reason why the *B-A* boundary coincides with E_F in the low-Θ limit regardless of the kind of the substrate is not very clear at present. At least, it is sure that such a structure of the resonance is suitable to gain a larger adsorption energy. The situation is similar to the diatomic molecule with the filled bonding state ϕ_b and the empty antibonding state ϕ_a as discussed in Sec. II.

It was shown in Sec. IV B that the Θ dependence of $d(\Theta)$ cannot be explained merely in terms of the conventional ionic-to-neutral change of adatoms due to the dipole-dipole interaction. Here, we show that the direct Na-Na interaction due to the orbital overlap instead plays a dominant role in the rapid decrease of $d(\Theta)$. First, we give a schematical explanation. Let us consider two Na atoms on the jellium surface. When they are well separated, the *B-A* boundary in $\mu_a(\varepsilon,\Theta)$ for each atomic resonance ϕ_i ($i=1,2$) coincides with E_F. Thus each atom has the largest $d(\Theta)$ by the maximum use of the bonding states polarized toward the interface [Fig. 12(a)]. With the decreasing Na-Na distance, the two atomic resonances split into the bonding (m_1) and antibonding (m_2) molecular resonances because of the increase of the transfer energy between the two sites. In this case, part of the strong antibonding states polarized toward the vacuum is occupied for m_1, whereas part of the bonding states is unoccupied for m_2 [Fig. 12(b)]. The two effects work cooperatively to decrease the induced dipole moment per adatom drastically. These effects can be seen only indirectly in Fig. 7: the amplitude of $\mu_a(\varepsilon,\Theta)$ below E_F becomes smaller, and the *B-A* boundary shifts slightly downward with increasing Θ. To prove the above-mentioned mechanism more directly, we decompose $\mu_a(\varepsilon,\Theta)$ in $\mathbf{k}$ space. Figure 13 shows the $\mathbf{k}$-resolved dipole DOS, $\mu_a(\mathbf{k},\varepsilon,\Theta)$ for the Na adlayer on jellium ($r_s=2$) at $a_{\parallel}=8.5$ a.u. along the $\bar{\Gamma}$-$\bar{K}$ line. The bonding (m_1) and antibonding (m_2) molecular resonances in Fig. 12 correspond to the $\bar{\Gamma}$ and $\bar{K}$ points, respectively. The *B-A* boundary in $\mu_a(\mathbf{k},\varepsilon,\Theta)$ disperses upward with increasing $\mathbf{k}$, corresponding to the energy dispersion of the resonance as shown in Fig. 10. It is seen that the strong antibonding resonance is actually mostly occupied at $\bar{\Gamma}$, whereas part of the bonding states are unoccupied at $\bar{K}$. This result is fully in accord with the qualitative explanation in Fig. 12.

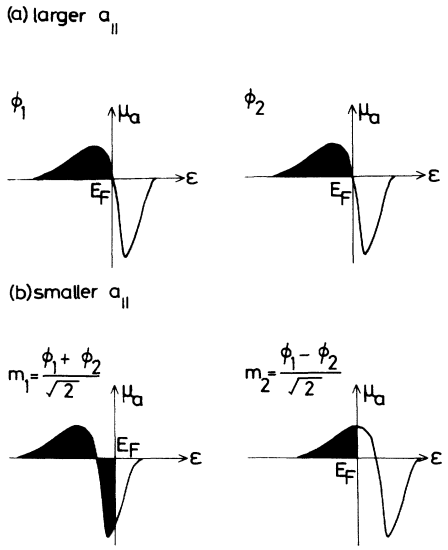

FIG. 12. Schematic illustration of the electronic structure of two alkali-metal adatoms when the orbital overlap of the two atoms is (a) small and (b) large.

The mechanism for the decrease of $d(\Theta)$ presented in

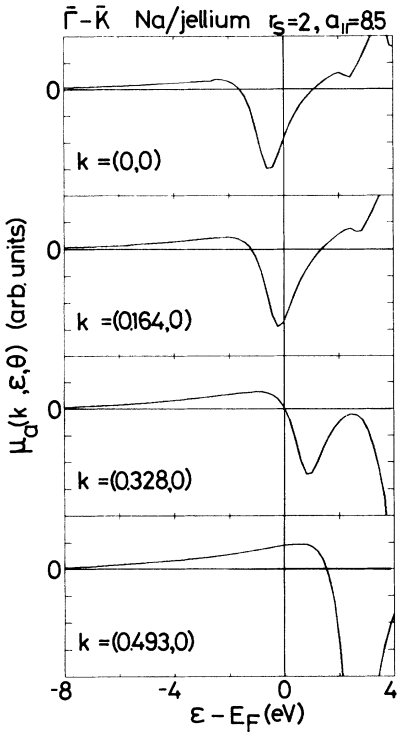

FIG. 13. $\mu_a(\mathbf{k},\varepsilon,\Theta)$ for the hexagonal Na adlayer with $a_{\parallel}=8.5$ a.u. on the jellium with $r_s=2$ along $\bar{\Gamma}$-$\bar{K}$ in the hexagonal surface Brillouin zone.

the above may be summarized as the weakening of the adatom-substrate bonding which follows the strengthening of the adatom-adatom bond. It is well known that the adsorption energy of the alkali-metal atom decreases substantially with increasing Θ. The above results suggest that there should be a close correlation between the decrease of $d(\Theta)$ and that of the adsorption energy with increasing Θ. Terakura[56] proposed that the mechanism can be also regarded as one example of the Heine's $\sqrt{N}$ theorem,[57] which says that the strength of the metallic bond between the atom under consideration and a neighboring one scales as $1/\sqrt{N}$, where N is the number of the surrounding atoms. In the present case, the increase in the number of neighboring adatoms weakens the adatom-substrate bond and consequently polarization of the adatom charge toward the interface, since part of the bond charge flows to the adatom-adatom bonds.

As stated in the Introduction, the jellium substrate is a good model for simple metals such as Al, but cannot describe the localized d states of transition metals. As was shown for the W and Mo substrates,[20,21] these d states hybridize with the alkali-metal s and p states, and also with the alkali-metal d states for heavier alkali-metals (K, Rb, and Cs), and contribute to E_c and $d_3(\Theta)$ [Eq. (3)]. Hence, some of the conclusions concerning the Θ dependence of the B-A boundary, E_c, and $d_3(\Theta)$ in the present paper may be affected by such additional adatom-substrate interactions. Further study is necessary in this direction.

V. SUMMARY

The aim of the present paper was to refine the results in I, where there was some ambiguity in calculated quantities such as the adatom DOS because of the slab approximation for the metal substrate. In the present work, we studied the electronic structure of alkali-metal adlayers on the semi-infinite jellium substrate as functions of the coverage and the r_s parameter of the jellium substrate by a first-principles method within the local-density-functional theory. The important results obtained are as follows. (1) In spite of the large potential lowering in the vacuum, the s-part of the adatom potential is insensitive to Θ by virtue of the efficient screening of the metallic substrate. (2) Therefore the filled part of the DOS in an adatom shows little depolarization shift, and is rather insensitive to Θ. (3) The charge state of the adatom, if simply defined by the area of the occupied part of the adatom DOS is close to the corresponding one for the isolated monolayer even for a small atomic sphere which contains only less than 0.1 electrons. (4) For all the substrates, the bonding-antibonding boundary with respect to the A-S bonding coincides with E_F at the lowest Θ, which suggests the important role of the covalent interaction in the A-S bond as well as of the interatomic polarization term in the adatom dipole moment. (5) The rapid decrease of the adatom dipole moment with increasing Θ is caused by the direct adatom-adatom interaction due to the orbital overlap, which leads to the stronger adatom-adatom bond and concomitantly to the weaker adatom-substrate bonding, more dominantly than the Θ-dependent charge transfer due to the indirect dipole-dipole interaction.

ACKNOWLEDGMENTS

The author is very grateful to Professor K. Terakura for valuable discussions. He is indebted to Dr. S. Blügel for allowing him to use his convergence method before publication. He thanks Dr. A. Liebsch and Dr. B. N. J. Persson for stimulating discussions on the present subject. Part of the present work is supported by a Grant-in-Aid for Scientific Research on Priority Areas from the Ministry of the Education, Science and Culture.

[1]K. H. Kingdon and I. Langmuir, Phys. Rev. **21**, 380 (1923); J. B. Taylor and I. Langmuir, *ibid.* **44**, 423 (1933).
[2]H. P. Bonzel, Surf. Sci. Rep. **8**, 43 (1987).
[3]T. Aruga and Y. Murata, Prog. Surf. Sci. **31**, 61 (1989).
[4]*Physics and Chemistry of Alkali Adsorption,* edited by H. P. Bonzel, A. M. Bradshaw, and G. Ertl (Elsevier, Amsterdam, 1989).
[5]J. Cousty, R. Riwan, and P. Soukiassian, J. Phys. (Paris) **46**, 1693 (1985); S. A. Lindgren and L. Wallden, Phys. Rev. B **22**, 5969 (1980).

[6]T. Aruga, H. Tochihara, and Y. Murata, Phys. Rev. Lett. **53**, 372 (1984); M. Tsukada, H. Ishida, and N. Shima, *ibid.* **53**, 376 (1984).

[7]H. Ishida and M. Tsukada, Surf. Sci. **169**, 225 (1986); D. M. Newns, Phys. Lett. **38A**, 341 (1972); M. Nakayama, T. Kato, and K. Ohtomi, Solid State Commun. **50**, 409 (1984).

[8]H. P. Bonzel, J. Vac. Sci. Technol. A **2**, 866 (1984).

[9]W. Eberhardt, F. M. Hoffman, R. de Paola, D. Heskett, I. Strathy, and E. W. Plummer, Phys. Rev. Lett. **54**, 1856 (1985).

[10]N. D. Lang, S. Holloway, and J. K. Nørskov, Surf. Sci. **150**, 24 (1985); P. J. Feibelman and D. R. Hamman, *ibid.* **149**, 48 (1985).

[11]H. W. K. Tom, C. M. Mate, X. D. Zhu, J. E. Crowell, Y. R. Shen, G. A. Somorjai, Surf. Sci. **172**, 466 (1986).

[12]K. J. Song, D. Heskett, H. L. Dai, A. Liebsch, E. W. Plummer, Phys. Rev. Lett. **61**, 1380 (1988).

[13]A. Liebsch, Phys. Rev. B **40**, 3421 (1989).

[14]K. W. Jacobsen and J. K. Nørskov, Phys. Rev. Lett. **60**, 2496 (1988).

[15]H. Ishida, Phys. Rev. B **38**, 8006 (1988).

[16]N. D. Lang and W. Kohn, Phys. Rev. B **3**, 1215 (1971).

[17]W. Kohn and L. J. Sham, Phys. Rev. **140**, A1133 (1965).

[18]P. Hohenberg and W. Kohn, Phys. Rev. **136**, B874 (1964).

[19]R. W. Gurney, Phys. Rev. **47**, 479 (1935).

[20]E. Wimmer, A. J. Freeman, M. Weinert, H. Krakauer, J. R. Hiskes, and A. M. Karo, Phys. Rev. Lett. **48**, 1128 (1982).

[21]E. Wimmer, A. J. Freeman, J. R. Hiskes, and A. M. Karo, Phys. Rev. B **28**, 3074 (1983); S. R. Chubb, E. Wimmer, A. J. Freeman, J. R. Hiskes, and A. M. Karo, *ibid.* **36**, 4112 (1987).

[22]P. Soukiassian, R. Riwan, J. Lecante, E. Wimmer, S. R. Chubb, and A. J. Freeman, Phys. Rev. B **31**, 4911 (1985).

[23]D. M. Riffe, G. K. Wertheim, and P. H. Citrin, Phys. Rev. Lett. **64**, 57 (1990).

[24]C. Astaldi, P. Rudolf, and S. Modesti, Solid State Commun. **75**, 847 (1990).

[25]N. D. Lang and A. R. Williams, Phys. Rev. B **18**, 615 (1978).

[26]N. D. Lang and A. R. Williams, Phys. Rev. B **16**, 2408 (1977).

[27]H. Hjelmberg, O. Gunnarsson, and B. I. Lundqvist, Surf. Sci. **68**, 158 (1977); O. Gunnarsson, H. Hjelmberg, and J. K. Nørskov, Phys. Scr. **22**, 165 (1980).

[28]H. Ishida, Phys. Rev. B **39**, 5492 (1989).

[29]H. Ishida, Phys. Rev. B **40**, 1341 (1989); Phys. Rev. Lett. **63**, 1535 (1989).

[30]S. Ciraci and I. P. Batra, Phys. Rev. Lett. **56**, 877 (1986); Phys. Rev. B **37**, 2955 (1988).

[31]R. V. Kasowski and M. H. Tsai, Phys. Rev. Lett. **60**, 546 (1988).

[32]H. Ishida and K. Terakura, Phys. Rev. B **40**, 11534 (1989).

[33]A. C. Hewson and D. M. Newns, Jpn. J. Appl. Phys. Suppl. **2**, 121 (1974).

[34]According to Ref. 25, the Na-induced dipole moment is 3.3 D at the equilibrium distance ($D_{as}=3.1$ a.u.), while it is 1.9 D when the adatom is on the image plane ($D_{as}=1.6$ a.u.).

[35]J. P. Muscat and D. M. Newns, J. Phys. C **7**, 2630 (1974).

[36]See also, H. Ishida and K. Terakura, Phys. Rev. B **38**, 5752 (1988).

[37]P. A. Serena and N. Garcia, Surf. Sci. **189/190**, 232 (1987); R. Wu, K. Chen, D. Wang, and N. Wang, Phys. Rev. B **38**, 3180 (1988); N. D. Lang, *ibid.* **4**, 4234 (1971).

[38]J. E. Inglesfield, J. Phys. C **14**, 3795 (1981).

[39]J. E. Inglesfield and G. A. Benesh, Phys. Rev. B **37**, 6682 (1988); G. A. Benesh and J. A. Inglesfield, J. Phys. C **17**, 1595 (1984).

[40]J. E. Inglesfield, Surf. Sci. **188**, L701 (1987); G. C. Aers and J. E. Inglesfield, *ibid.* **217**, 367 (1989).

[41]The expansion coefficients $n(\mathbf{G},m)$, $n_a(\mathbf{G},m)$, and $n_J(\mathbf{G},m)$ are not uniquely determined, since the basis functions $\cos(\mathbf{k}_m z)$ $(m \geq 0)$ are not orthogonal in the interval, $b_1 \leq z \leq b_2$. A different choice of these coefficients leads to different $n_t(\mathbf{G},z)$ in the unphysical regions $0 \leq z \leq b_1$ and $b_2 \leq z \leq l$.

[42]G. B. Bachelet, D. R. Hamman, and M. Schlüter, Phys. Rev. B **26**, 4199 (1982).

[43]The sign was misprinted as "positive" in Ref. 28.

[44]S. Blügel (unpublished).

[45]Lang and Williams (Ref. 25) obtained $D_{as}=3.1$ a.u. in the low Θ limit for the jellium substrate with $r_s=2$. Because of the pseudopotential calculation which neglects the core polarization, the present calculational scheme would obtain slightly smaller D_{as} values at low coverages.

[46]The second term of Eq. (17) is the density of states of the clean jellium surface calculated in the same Na sphere. The definition of $\rho_a(\varepsilon,\Theta)$ coincides with that of Ref. 25 if the volume integration in Eq. (17) is performed in the entire unit cell instead of a small Na sphere.

[47]The magnitude of the depolarization shift depends crucially on the distance between the centroid of the orbital and the image plane D [see, B. N. J. Persson and H. Ishida, Phys. Rev. B **42**, 3171 (1990)]. The depolarization shift for the occupied states polarized toward the metal is smaller than that of the s-p_z hybridzed peak because of smaller D.

[48]This was also the case in I. See Fig. 7 of I.

[49]B. N. J. Persson and L. H. Dubois, Phys. Rev. B **39**, 8220 (1989).

[50]J. P. Muscat and D. M. Newns, Solid State Commun. **11**, 737 (1972); J. P. Muscat and I. P. Batra, Phys. Rev. B **34**, 2889 (1986); D. Drakova, G. Doyen, and R. Hübner, J. Chem. Phys. **89**, 1725 (1988).

[51]K. Horn, A. Hohlfeld, J. Somers, Th. Linder, P. Hollins, and A. M. Bradshaw, Phys. Rev. Lett. **61**, 2488 (1988).

[52]See also, K.-H. Frank, H.-J. Sagner, and D. Heskett, Phys. Rev. B **40**, 2767 (1989); D. Heskett, K.-H. Frank, E. E. Koch, and H.-J. Freund, *ibid.* **36**, 1276 (1987).

[53]B. A. Benesh and J. R. Hester, Surf. Sci. **194**, 567 (1988).

[54]E. Wimmer, J. Phys. F **13**, 2313 (1983).

[55]B. Woratschek, W. Sesselman, J. Küppers, G. Ertl, and H. Haberland, Phys. Rev. Lett. **55**, 1231 (1985).

[56]K. Terakura (unpublished).

[57]V. Heine, in *Many-Atom Interactions in Solids,* edited by R. M. Nieminen, M. J. Puska, and M. J. Manninen (Springer, Berlin, 1990).